Non-parametric inference of impurity transport coefficients in the ASDEX Upgrade tokamak

T. Nishizawa[1], R. Dux[1], R. M. McDermott[1], C. Schuster[1,2], M. Cavedon[1], E. Wolfrum[1], U. von Toussaint[1], A. Jansen Van Vuuren[3,4], D. J. Cruz-Zabala[3,4], P. Cano-Megias[4,5], and the ASDEX Upgrade Team

[1]Max-Planck-Institut für Plasmaphysik, [2]Physik-Department E28, Technische Universität München,
[3]Dept. of Atomic, Molecular and Nuclear Physics, University of Seville,
[4]Centro Nacional de Aceleradores, [5]Dept. of Energy Engineering, University of Seville

This work has been carried out within the framework of the EUROfusion Consortium and has received funding from the Euratom research and training programme 2014-2018 under grant agreement No 633053. The views and opinions expressed herein do not necessarily reflect those of the European Commission.

outline

- introduction
- impurity transport coefficient measurements
- Summary and conclusions

Parametric vs Non-parametric inference

Parametric inference (conventional)

Consider a case where we have only 3 spatial points.

Bayes Theorem

$$p(\vec{\theta}|\vec{D},\vec{I}) \propto p(\vec{D}|\vec{\theta},\vec{I})p(\vec{\theta}|\vec{I})$$

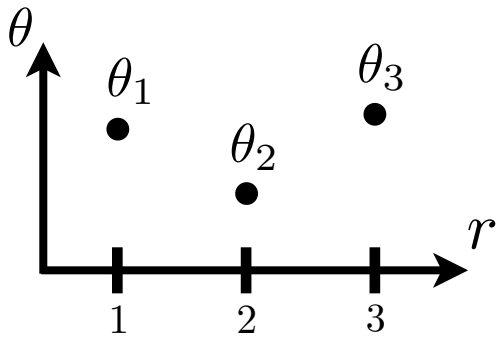

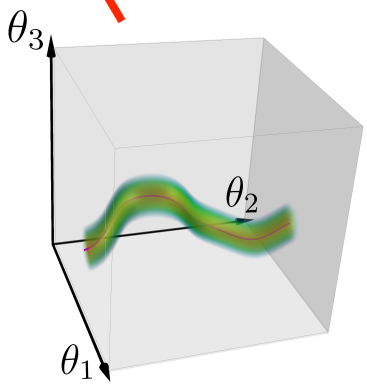

ill-posed likelihood

Each spatial point has its own axis (degree of freedom).

Parametric vs Non-parametric inference

Parametric inference (conventional)

Consider a case where we have only 3 spatial points.

Bayes Theorem

$$p(\vec{\theta}|\vec{D},\vec{I}) \propto p(\vec{D}|\vec{\theta},\vec{I})p(\vec{\theta}|\vec{I})$$

Use a linear function to represent a profile

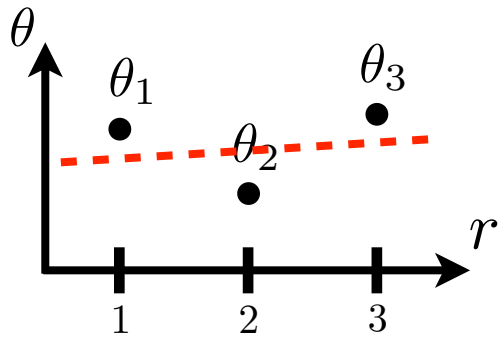

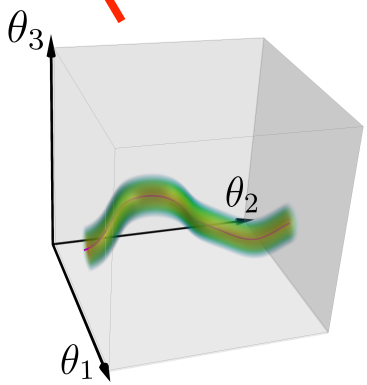

ill-posed likelihood

Each spatial point has its own axis (degree of freedom).

Parametric vs Non-parametric inference

Parametric inference (conventional)

Consider a case where we have only 3 spatial points.

Use a linear function to represent a profile

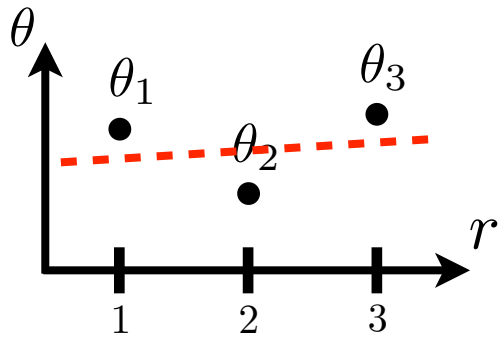

Bayes Theorem

$$p(\vec{\theta}|\vec{D},\vec{I}) \propto p(\vec{D}|\vec{\theta},\vec{I})p(\vec{\theta}|\vec{I})$$

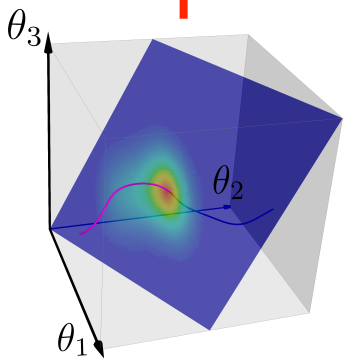

posterior obtained by a parametric approach

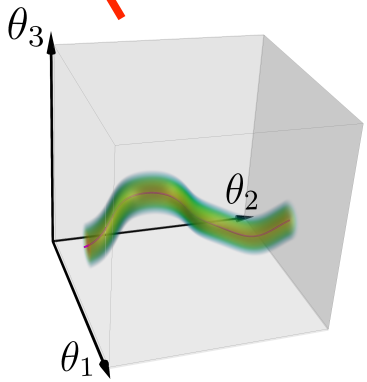

ill-posed likelihood

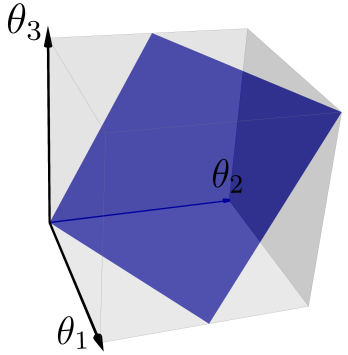

Surface defined by linear functions

Non-parametric inference

Consider a case where we have only 3 spatial points.

Each spatial point has its own degree of freedom

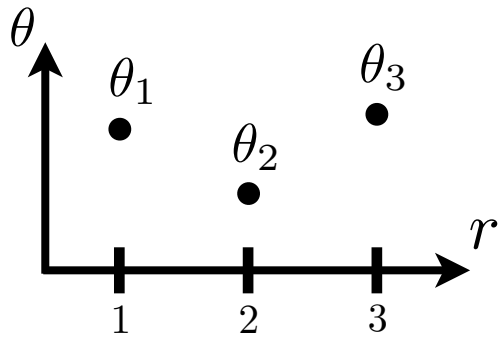

Bayes Theorem

$$p(\vec{\theta}|\vec{D},\vec{I}) \propto p(\vec{D}|\vec{\theta},\vec{I})p(\vec{\theta}|\vec{I})$$

3D distribution

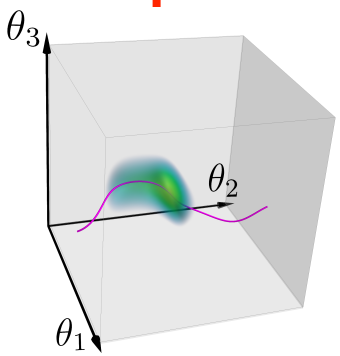

posterior obtained by a **non**-parametric approach

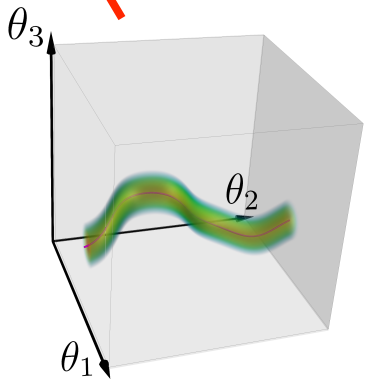

ill-posed likelihood

3D distribution

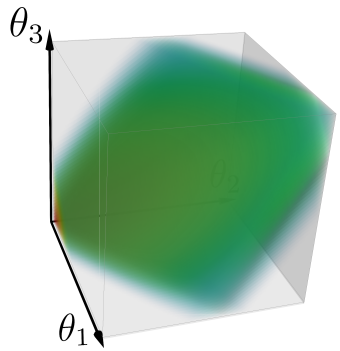

Smoother profiles have higher probabilities

e.g., Gaussian process

Non-parametric inference

advantage

preserves the original dimension

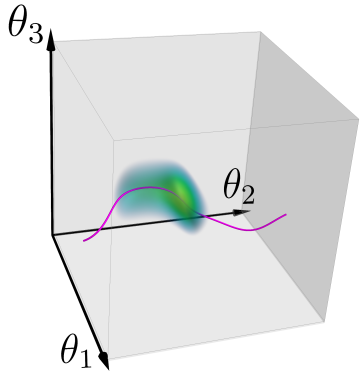

- Comprehensive search in the solution space
  e.g., profiles are not limited to piecewise-connected cubic functions

disadvantage

Many many parameters !

- Large degrees of freedom often require **unpractical computational resource**
  exception: analytical solution of the posterior is available
  ne and Te can be inferred without a computational challenge
  by using a non-parametric approach

M.A. Chilenski, et.al., Nucl. Fusion **55** (2015), A. Ho, et.al., Nucl. Fusion **59** (2019)

MCMC or nested sampling

Non-parametric inference

advantage

preserves the original dimension

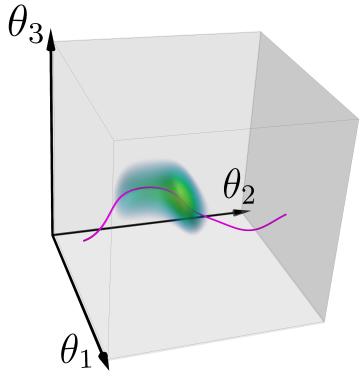

- Comprehensive search in the solution space
e.g., profiles are not limited to piecewise-connected cubic functions

disadvantage

Many many parameters !

- Large degrees of freedom often require **unpractical computational resource**

address this!

This work tries to make the problem trackable by optimizing the experimental setup and the model

outline

- introduction
- impurity transport coefficient measurements
- Summary and conclusions

CXRS measurements of a static plasma

Quasi-static Type-III ELMy H-mode (No time evolution of impurity distribution)

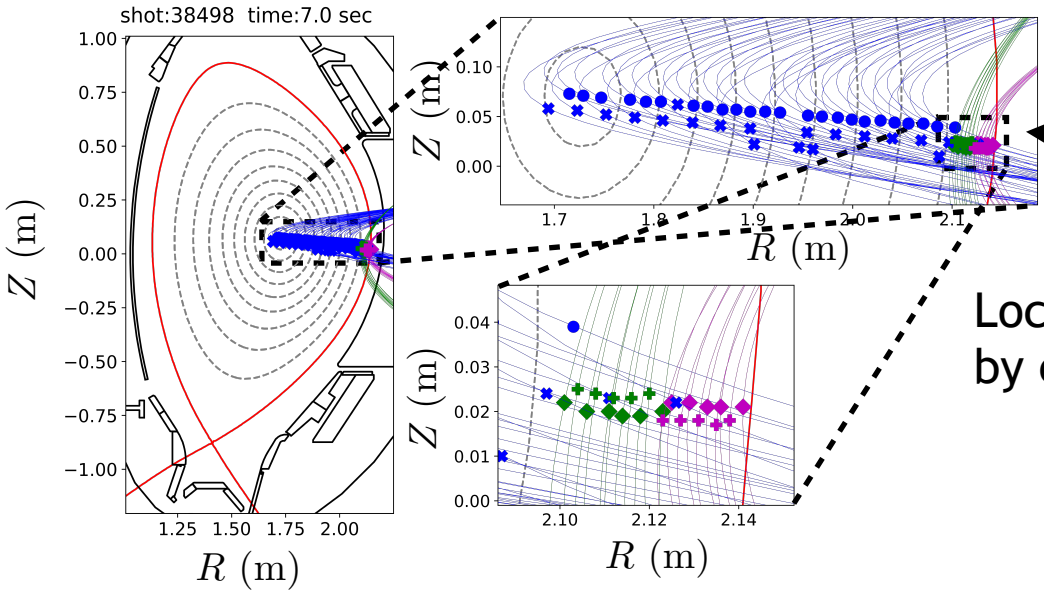

Neutral beam injection

Local impurity emission is induced by charge-exchange reactions

The density profiles of Ne^{10+}, C^{6+}, and $\underline{Ne^{8+}+O^{8+}}$ are measured.

Only the sum of these two is available due to the overlapping lines.

Ne, O, and C are assumed to have the same transport coefficients.

Why using the quasi-static plasma

Note

Only the ration of v to D can be determined!

$$n_z(r) \propto \exp\left(\int^r \frac{v}{D} dr'\right)$$

This is true only when all impurity ions are in the fully ionized state

→ By simultaneously measuring different charge states, the diffusion coefficient and the convection velocity can still be decoupled.

For a steady-state, impurity profiles can be analytically solved for given D and v without evaluating the time-evolution of the system.

→ leads to **a significant reduction in the computational cost**

We used MCMC.

$$\begin{bmatrix} \vec{n}_1 \\ \vec{n}_2 \\ \vec{n}_3 \\ \vdots \\ \vec{n}_{Z-1} \\ \vec{n}_Z \end{bmatrix} = \hat{M}^{-1} \begin{bmatrix} n_{1,N+1}\vec{u} \\ n_{2,N+1}\vec{u} \\ n_{3,N+1}\vec{u} \\ \vdots \\ n_{Z-1,N+1}\vec{u} \\ n_{Z,N+1}\vec{u} \end{bmatrix}$$

$$\hat{M} = \begin{bmatrix} \hat{1}+\hat{B}_1 & -\hat{A}_2 & 0 & 0 & \cdots & 0 & 0 & 0 \\ -\hat{B}_1 & \hat{1}+\hat{A}_2+\hat{B}_2 & -\hat{A}_3 & 0 & \cdots & 0 & 0 & 0 \\ 0 & -\hat{B}_2 & \hat{1}+\hat{A}_3+\hat{B}_3 & -\hat{A}_4 & \cdots & 0 & 0 & 0 \\ \vdots & \vdots & 0 & \vdots & \ddots & \vdots & \vdots & \vdots \\ 0 & 0 & 0 & 0 & \cdots & \hat{B}_{Z-2} & \hat{1}+\hat{A}_{Z-1}+\hat{B}_{Z-1} & -\hat{A}_Z \\ 0 & 0 & 0 & 0 & \cdots & 0 & -\hat{B}_{Z-1} & \hat{1}+\hat{A}_Z \end{bmatrix}$$

Analytical solution is available!

Inference model

When constructing the model, parameterization is chosen such that it facilities the use of the NUTS sampler (Pymc3).

prior distributions

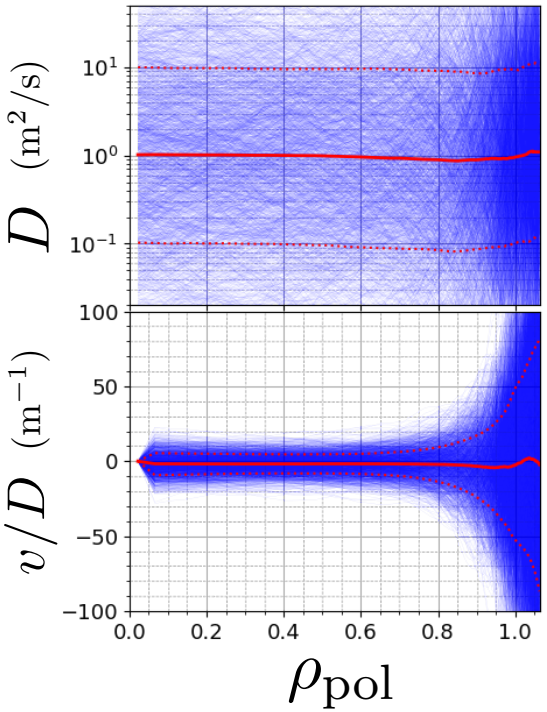

Start with the Gaussian process

$$p(\vec{D}|\hat{\Sigma}) \propto \exp\left(-\frac{1}{2}\vec{\theta}^{\mathrm{T}}\hat{\Sigma}^{-1}\vec{\theta}\right)$$

$$\vec{\theta}^{\mathrm{T}} = [\log_{10} D_1, \log_{10} D_2, \cdots, \log_{10} D_N],$$

$$\hat{\Sigma}_{n,n'} = \sigma_D^2 \exp\left(-\frac{(r_n - r_{n'})^2}{2l_{\mathrm{co}}^2}\right),$$

$$p(\vec{\psi}|\hat{\Omega}) \propto \exp\left(-\frac{1}{2}\vec{\psi}^{\mathrm{T}}\hat{\Omega}^{-1}\vec{\psi}\right),$$

$$\hat{\Omega}_{n,n'} = F^2 \exp\left(-\frac{(r_n - r_{n'})^2}{2l_{\mathrm{co}}^2}\right),$$

$$\sum_{i=1}^{n} \frac{v_i}{D_i}\Delta r_i = (\psi_n - \psi_1) - (F + \psi_n - \psi_1)\cdot\frac{r_n}{r_N}$$

Impurity transport coefficients D and v

Type-III ELMy H-mode

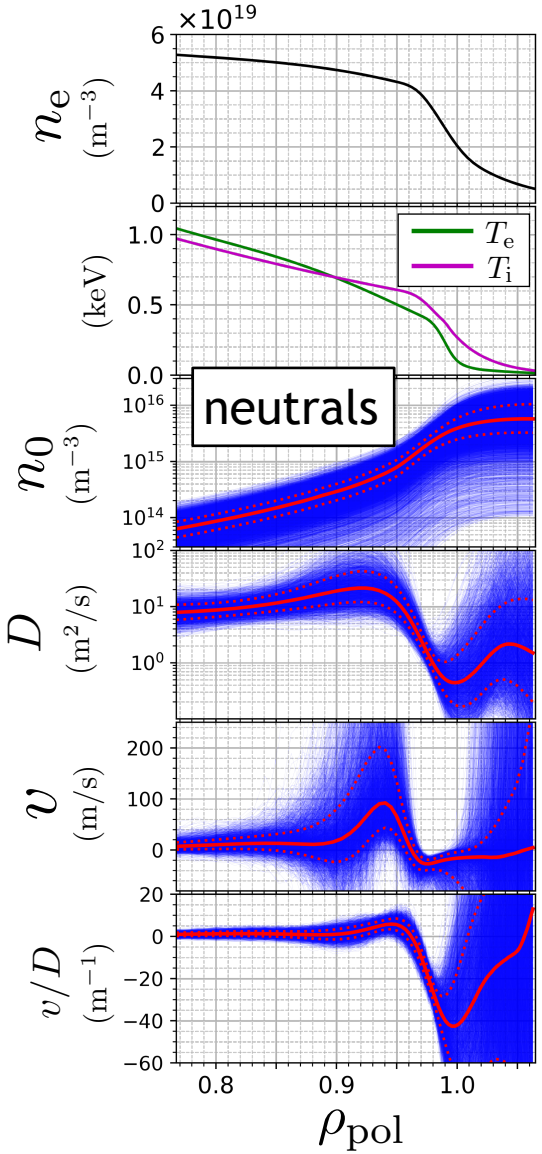

CX with the thermal neutrals is taken into account

$$p(\vec{n}_0,\vec{T}_0|E_{0,\mathrm{wall}},n_{0,\mathrm{wall}})p(E_{0,\mathrm{wall}})p(n_{0,\mathrm{wall}}),$$
$$p(E_{0,\mathrm{wall}}) \propto 1/E_{0,\mathrm{wall}} \quad 10\ \mathrm{eV} \leq E_{0,\mathrm{wall}} \leq 120\ \mathrm{eV},$$
$$p(n_{0,\mathrm{wall}}) \propto 1/n_{0,\mathrm{wall}} \quad 10^4\ \mathrm{m}^{-3} \leq n_{0,\mathrm{wall}} \leq 10^{18}\ \mathrm{m}^{-3}.$$

A Monte-Carlo code determines the profiles from the edge conditions.

R. Dux, et.al. NF (2020), F. Sciortino, et.al. NF (2021) showed neutrals cannot be neglected.

Impurity transport coefficients D and v

Type-III ELMy H-mode

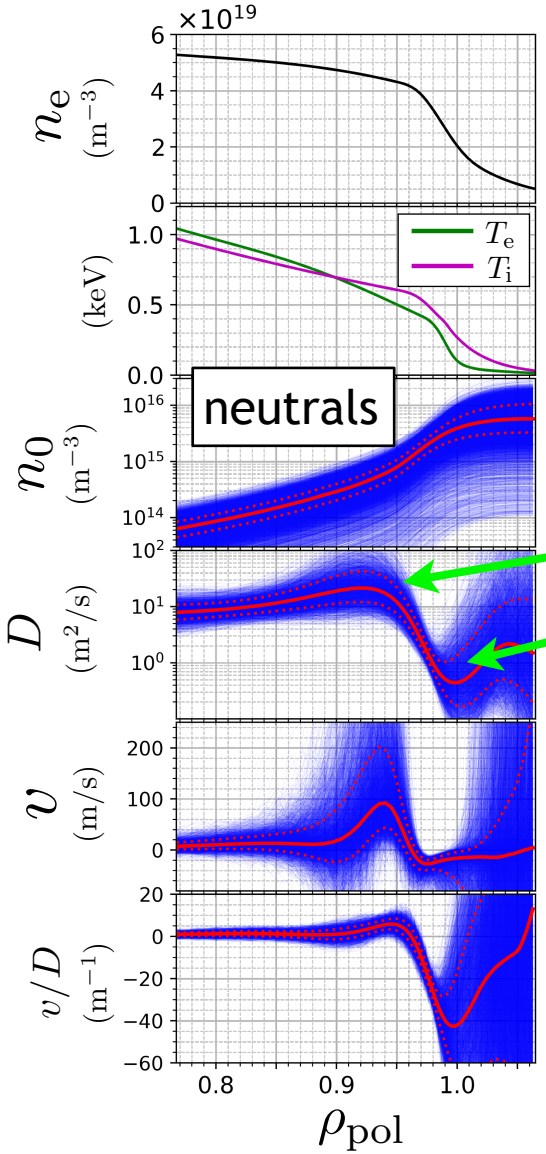

CX with the thermal neutrals is taken into account

$$p(\vec{n}_0,\vec{T}_0|E_{0,\mathrm{wall}},n_{0,\mathrm{wall}})p(E_{0,\mathrm{wall}})p(n_{0,\mathrm{wall}}),$$
$$p(E_{0,\mathrm{wall}}) \propto 1/E_{0,\mathrm{wall}} \quad 10\ \mathrm{eV} \leq E_{0,\mathrm{wall}} \leq 120\ \mathrm{eV},$$
$$p(n_{0,\mathrm{wall}}) \propto 1/n_{0,\mathrm{wall}} \quad 10^4\ \mathrm{m}^{-3} \leq n_{0,\mathrm{wall}} \leq 10^{18}\ \mathrm{m}^{-3}.$$

A Monte-Carlo code determines the profiles from the edge conditions.

R. Dux, et.al. NF (2020), F. Sciortino, et.al. NF (2021) showed neutrals cannot be neglected.

$D \sim 20\ \mathrm{m/s^2}$ just inside the pedestal

$D < 1\ \mathrm{m/s^2}$ at the pedestal

Impurity transport coefficients D and v

Type-III ELMy H-mode

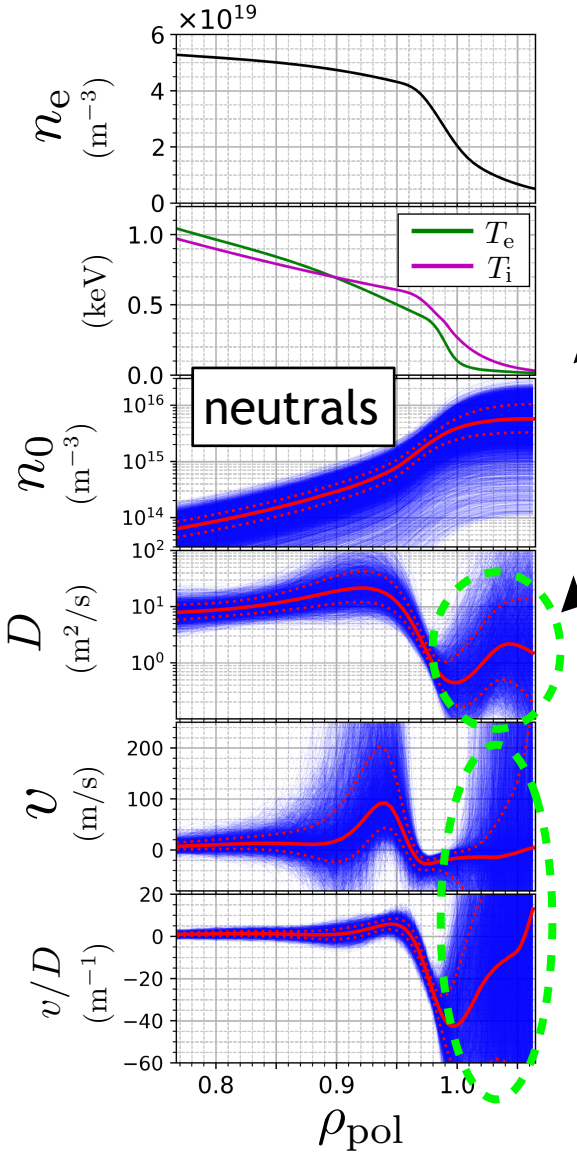

CX with the thermal neutrals is taken into account

$$p(\vec{n}_0,\vec{T}_0|E_{0,\mathrm{wall}},n_{0,\mathrm{wall}})p(E_{0,\mathrm{wall}})p(n_{0,\mathrm{wall}}),$$
$$p(E_{0,\mathrm{wall}}) \propto 1/E_{0,\mathrm{wall}} \quad 10\ \mathrm{eV} \leq E_{0,\mathrm{wall}} \leq 120\ \mathrm{eV},$$
$$p(n_{0,\mathrm{wall}}) \propto 1/n_{0,\mathrm{wall}} \quad 10^4\ \mathrm{m}^{-3} \leq n_{0,\mathrm{wall}} \leq 10^{18}\ \mathrm{m}^{-3}.$$

A Monte-Carlo code determines the profiles from the edge conditions.

No CXRS data available in the SOL

prior distribution

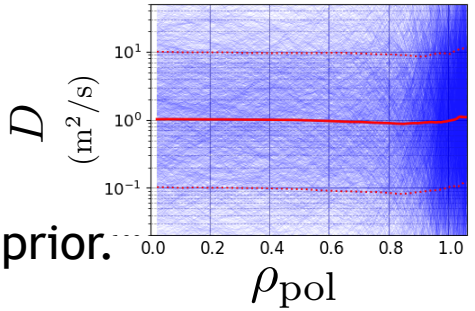

Distribution is close to the prior.

Very wide distributions.
In a non-parameter inference, each spatial grid has its own degree of freedom. If the likelihood fails to provide meaningful information, only the prescribed smoothing conditions provide constraints.

Summary and Conclusions

- Complete search in the solution space is possible through a non-parametric approach
  (Each spatial point keeps its own degree of freedom)

- D(diffusion coefficient) and v(convection velocity) can be measured without modulating the impurity profile by simultaneously observing multiple impurity charge states

- An analytical solution for impurity profiles significantly reduces the computation cost and makes a non-parametric approach possible.

- The profiles of D(diffusion coefficient) and v(convection velocity) in the edge of a Type-III ELMy H-mode plasma are successfully obtained.